Received August 2002
Revised January 2003
Accepted January 2003

Computation of combined turbulent convective and impingement heat transfer

Bengt Sundén, Rongguang Jia and Andreas Abdon
Division of Heat Transfer, Lund Institute of Technology, Lund, Sweden

Keywords *Force measurement, Convection, Cooling, Turbulence, Finite volume methods*

Abstract *Impingement and forced convection are preferable methods for cooling gas turbine components. However, influences of various design parameters like crossflow and surface enlargements (like ribs) are not well understood. Thus there is a request for reliable and cost-effective computational prediction methods, due to the experimental difficulties. Such methods could be based on the numerical solution of the Reynolds-averaged Navier-Stokes equations, the energy equation and models for the turbulence field. This paper describes some recent advances and efforts to develop and validate computational methods for simulation of impingement and forced convection cooling in generic geometries of relevance in gas turbine cooling. Single unconfined round air jets, confined jets with crossflow, and three-dimensional ribbed ducts are considered. The numerical approach is based on the finite volume method and uses a co-located computational grid. The considered turbulence models are all the so-called low Reynolds number models. Our recent investigations show that linear and non-linear two-equation turbulence models can be used for impinging jet heat transfer predictions with reasonable success. However, the computational results also suggest that an application of a realizability constraint is necessary to avoid over-prediction of the stagnation point heat transfer coefficients. For situations with combined forced convection and impingement cooling it was revealed that as the crossflow is squeezed under the jet, the heat transfer coefficient is reduced. In addition, inline V-shaped 45° ribs pointing upstream performed superior compared to those pointing downstream and transverse ribs.*

Nomenclature

e	= rib width and height (square rib)	$\rho c_p \overline{u'\phi'}$	= turbulent heat fluxes
H	= nozzle-to-wall distance	W_{ij}	= mean vorticity
k	= turbulent kinetic energy	y^+	= dimensionless distance to the wall
Nu	= local Nusselt number	ε	= dissipation rate
Re	= Reynolds number	ν_T	= turbulent kinematic viscosity
$-\overline{\rho u'v'}$	= turbulent stresses		

Introduction

Among various cooling methods of gas turbine components, impingement and forced convection cooling is preferable due to improved cycle efficiency and reduced emission levels. This method is applied for cooling the walls of low

The Swedish National Energy Agency (STEM) and the National Gas Turbine Center financially supported this work.

International Journal of Numerical Methods for Heat & Fluid Flow
Vol. 14 No. 1, 2004
pp. 116-133

0961-5539
DOI 10.1108/09615530410511667

emission combustors, as shown in Figure 1(a), and for internal cooling of the leading edge of guide vanes and gas turbine blades, as shown in Figure 1(b). However, influences of various design parameters like crossflow and surface enlargements (like ribs) are not well understood. Reliable engineering design methods for complex geometries and flow systems are not available and only a very limited amount of experimental data exist. In addition, experiments on real applications are cumbersome, very costly and not attractable at least in terms of detailed and fundamental investigations. Thus there is a request for reliable and cost-effective computational prediction methods based on numerical solution of the governing equations for momentum and heat transport. Such methods could be based on the numerical solution of the Reynolds-averaged Navier-Stokes equations (RANS), the energy equation and models for the turbulence field.

A brief review on some of the previous efforts concerning impinging air jet heat transfer and RANS simulations is given. Several earlier investigations (Ashforth-Frost and Jambunathan, 1996; Behnia *et al.*, 1998; Craft *et al.*, 1993) have revealed that prediction of impinging jet heat transfer is a challenging task. Heyerichs and Pollard (1996) examined an impinging slot jet at a Reynolds number (based on the nozzle width) of 10,000 using a large number of two-equation linear turbulence models. The models utilized different near wall treatments including wall functions, a two layer (zonal) model and low Reynolds number (low-Re) models. The local heat transfer rates were in general in good agreement with experimental data, except when wall functions were applied. Hosseinalipour and Mujumdar (1995) performed a similar investigation at a slightly lower Reynolds number with satisfactory agreement. A configuration of three impinging slot jets was investigated by Seyedin *et al.* (1995) at Re = 6,000 using a low-Re k-ε model (Lam-Bremhorst)

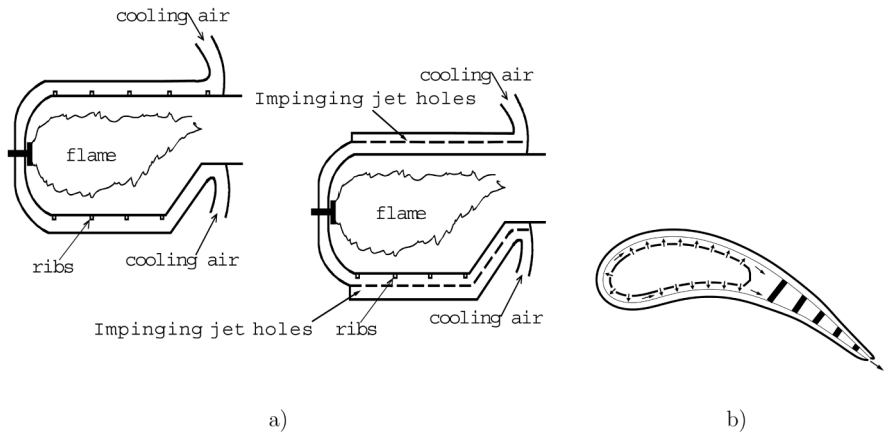

Note: The dashed lines mean the divider with holes to generate

Figure 1.
Schematic view of cooling of: (a) a combustor; and (b) a blade

and also a high Re wall function treatment. The results showed acceptable overall agreement but a large difference for the two approaches concerning stagnation heat transfer rates. Recently, Tzeng *et al.* (1999) simulated the same configuration for a number of low-Re k-ε models and good agreement with experimental data was established. In general, the investigations mentioned earlier suggest that impinging jet heat transfer is handled well by the popular two-equation models but the near wall treatment is crucial; wall functions tend to underpredict stagnation zone heat transfer rates. The poor performance of the wall functions is not surprising because they rest on assumptions of equilibrium flow conditions, which is typically found in flows parallel to walls at a dimensionless distance to the wall (y^+) of about 30. This leaves questions of how to distribute a suitable finite volume grid and demonstrate grid independence.

Heat transfer and fluid flow in 3D ribbed ducts is another challenging case, mainly due to the flow separation induced by negative pressure gradient, and secondary motion promoted by the anisotropy of the Reynolds stresses. Even in experiments, large contradictions exist, such as the goodness of the pointing direction of V-shaped ribs (Han *et al.*, 1991; Olsson and Sundén, 1998; Taslim *et al.*, 1996). Thus there is a need to employ accurate numerical methods to clarify this. Iacovides and Raisee (1999) carried out computations of periodic flow and heat transfer through stationary and rotating ducts of square cross-section with rib-roughened walls. They considered a zonal k-ε model, a low-Re k-ε model and a low-Re differential stress model. The low-Re differential stress model yields thermal predictions that are superior to those of low-Re k-ε model. Saidi and Sundén (2000) studied the turbulent convective heat transfer in 3D rib-roughened channels, using a simple eddy viscosity model (EVM) and an explicit algebraic stress model (EASM). As reported, the EASM has some superiority over the EVM in prediction of the velocity field, but showed similar ability in thermal simulation. More recently, Jang *et al.* (2001) employed a multi-block solver to study the heat and flow in two-pass channels with 60° ribs. In their study, the near-wall second-moment closure model is shown to predict the heat transfer more faithfully than the two-layer k-ε model. According to the available literature, however, no detailed data of experiments or numerical prediction for ducts roughened with V-shaped ribs has been reported to clarify the contradictions in experimental results from different researchers, which is important in understanding the fluid flow characteristics and heat transfer enhancement of this kind of turbulators. This paper also reports the authors' efforts to further improve the understanding of the internal cooling of turbine blades roughened with V-shaped ribs.

Objectives

This paper describes some recent advances and efforts to develop and validate computational methods for simulation of impingement and forced convection

cooling in generic geometries of relevance in gas turbine cooling. Turbulence modeling is a critical issue and it is known that the widely used linear two-equation models suffer from a too high generation of turbulence and thus heat transfer in stagnating flow fields. This problem may be eliminated or at least reduced by using more advanced formulations like full Reynolds stress equations or by application of a realizability constraint on the linear two-equation models. In recent years, non-linear formulations of the constitutive relations have emerged and the performance of the two-equation models has been improved. The main reasons for this improvement are the incorporation of variable coefficients in the stress-strain relationship (constitutive relation) and the ability to more adequately capture anistropy in the turbulent normal stresses. These features are believed to affect the predictions and will be discussed in this paper.

Problem statement

The geometries selected for the investigation are idealized to reveal the fundamental issues and enable validation of the considered models with available experimental data. Thus single unconfined round air jets, confined jets with crossflow, and three-dimensional ribbed ducts are considered.

The first test case investigated here is a single unconfined impinging round air ($Pr = 0.7$) jet (Re=23,000 and 70,000, $H/D = 2$). Figure 2(a) shows the computational domain which extends to $H + 8D$ and $H + 2D$ in the radial and axial directions, respectively. As the jets were fully developed flows in the reference experimental setups (Baughn *et al.*, 1991; Lytle and Webb, 1994; Yan, 1993), this is also used as inlet condition in the calculations. The inlet profiles of all variables were interpolated from a fully developed pipe flow using high numerical resolution. A constant (uniform) value of the temperature is used at the inlet. The free boundaries of the unconfined jets are subjected to a constant pressure condition, and a zero gradient condition for outgoing flow is used for the transported variables. Incoming ambient flow is designated constant variable values to achieve low or zero turbulence (different values were tested and showed no impact on predicted heat transfer distribution), and the temperature is set equal to the jet inlet temperature. Constant fluid properties are applied and the flow is regarded as incompressible in all the calculations. The thermal boundary condition at the bottom wall is a constant heat flux in accordance with the experiments while the other walls (pipe) are insulated.

The second test case is the simulation, based on the experiments of Oladiran (1981) who examined the effect of crossflow and jet inclination on impinging jet heat transfer. In the experiments a round jet issuing from a pipe was made to impinge on the bottom wall of a channel of rectangular cross-section. Figure 2(b) shows the computational domain. The close-up view of the grid close to the jet inlet is shown in Figure 2(c). The width (W) and height (H) of the channel were 26 and 6 pipe diameters (D), respectively. A crossflow was fed

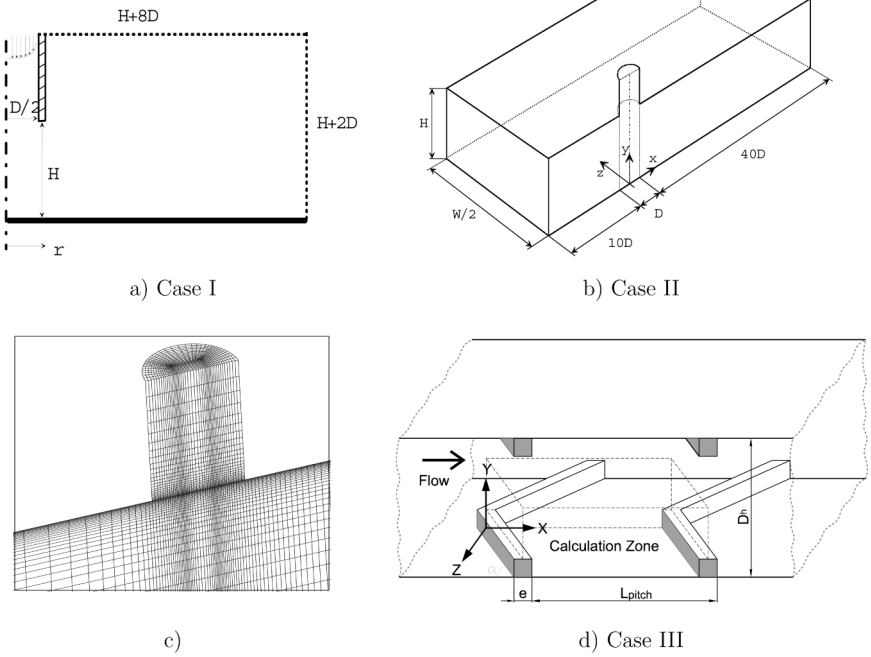

Figure 2.
Computational domain for (a) a circular impingement jet; (b) a circular jet issued into a cross flow; (c) close-up view of the computation grid of Case II; and (d) V-shaped ribbed duct

through the channel from a plenum chamber supplied with flow straightener. The distance between the plenum chamber and the channel was bridged by a connecting duct sufficiently long to yield a 1/15th power law velocity profile (Oladiran, 1981) in the duct outlet. As for the jet, the length of the pipe was 32*D* which should be sufficient to establish fully developed flow conditions at the outlet, and the Reynolds number, based on the jet pipe diameter, was kept constant at 32,500. The naphthalene sublimation technique (mass transfer and Chilton-Colburn analogy) was used to evaluate the bottom wall heat transfer, in the experiments of Oladiran (1981).

The boundary conditions for the second case are fully developed inlet profiles of jet and crossflow. These profiles, including turbulence variables, have been calculated separately. At the channel outlet, a zero gradient condition in the main flow direction is applied on all variables. A constant temperature is set at the bottom wall which corresponds to the boundary condition of the mass transfer experiments. The fluid properties are regarded as constant and the flow is incompressible in the experiments as well as in the simulations.

The third test case is the simulation of the heat transfer and fluid flow in a straight duct with in-line V-shaped ribs mounted on two opposite walls periodically, which is selected mainly for the clarification of the contradiction

between different experiments (Han *et al.*, 1991; Olsson and Sundén, 1998; Taslim *et al.*, 1996). The geometry is shown in Figure 2(d). The angle of a V-shaped rib can be 90 and 45°. The ratio of pitch to rib height (P/e) is equal to 10, and the ratio of rib height to hydraulic diameter (e/D) is 0.0625, which are chosen in accordance with Han *et al.* (1981). Owing to the periodic and symmetry properties of the geometry, the calculation domain is selected as indicated in Figure 2(d) to minimize the computational cost. The considered Reynolds numbers range from 14,000 to 35,000. Both the ribbed (including the surfaces of the ribs) and smooth walls were set as constant heat flux boundaries.

Governing equations and turbulence models

Governing equations

The governing equations to be solved are the continuity, momentum, and energy equations and the transport equations for the turbulent kinetic energy and dissipation added through the turbulence model.

$$\frac{\partial U_i}{\partial x_i} = 0 \tag{1}$$

$$\frac{\partial U_i}{\partial t} + \frac{\partial (U_j U_i)}{\partial x_j} = -\frac{1}{\rho}\frac{\partial P}{\partial x_i} + \frac{\partial}{\partial x_j}\left(2\nu S_{ij} - \overline{u_i' u_j'}\right) \tag{2}$$

$$\frac{\partial \Phi}{\partial t} + \frac{\partial (U_j \Phi)}{\partial x_j} = \frac{\partial}{\partial x_j}\left(\frac{\nu}{\mathrm{Pr}}\frac{\partial \Phi}{\partial x_j} - \overline{\phi' u_j'}\right) \tag{3}$$

where $\tau_{ij} = -\overline{u_i' u_j'}$ is known as the specific Reynolds stress tensor, and $-\overline{\phi' u_j'}$ is the specific turbulent fluxes. Both of these two terms need to be modeled. This is known as the closure problem of turbulence.

Turbulence models

The considered turbulence models are all the so-called low Reynolds number models (both linear and non-linear ones). A realizability constraint is applied on the linear models to prevent severe over-prediction of the heat transfer at stagnation points. The constraint puts a limit on the timescale for the turbulence field. Anisotropic formulations of the turbulent heat fluxes are discussed and some comparative results are considered.

The k-ε models. All the k-ε models use the following transport equations:

$$\frac{\partial k}{\partial t} + \frac{\partial (U_j k)}{\partial x_j} = \frac{\partial}{\partial x_j}\left[\left(\nu + \frac{\nu}{\sigma_k}\right)\frac{\partial k}{\partial x_j}\right] + P_\mathrm{k} - \varepsilon \tag{4}$$

$$\frac{\partial \varepsilon}{\partial t}+\frac{\partial (U_j \varepsilon)}{\partial x_j}=\frac{\partial}{\partial x_j}\left[\left(\nu+\frac{\nu}{\sigma_\varepsilon}\right)\frac{\partial \varepsilon}{\partial x_j}\right]+\frac{f_{\varepsilon 1}C_{\varepsilon 1}P_{\mathrm{k}}-f_{\varepsilon 2}C_{\varepsilon 2}\varepsilon}{T} \tag{5}$$

where $T=k/\varepsilon$ is the timescale and

$$P_{\mathrm{k}}=-\overline{u_i' u_j'}\frac{\partial U_i}{\partial x_j}$$

is the production of kinetic energy. The following expressions are valid for all the models:

$$S_{ij}=\frac{1}{2}\left(\frac{\partial U_i}{\partial x_j}+\frac{\partial U_j}{\partial x_i}\right),\quad W_{ij}=\frac{1}{2}\left(\frac{\partial U_i}{\partial x_j}-\frac{\partial U_j}{\partial x_i}\right) \tag{6}$$

$$\nu_t=f_\mu C_\mu k T \tag{7}$$

The linear model of Abe et al. (1994)

$$\tau_{ij}=-\overline{u_i' u_j'}=2\nu_t S_{ij}-\frac{2}{3}k\delta_{ij} \tag{8}$$

$$\begin{aligned} f_\mu &= \left(1-\mathrm{e}^{-\frac{y^*}{14}}\right)^2\left(1+5\mathrm{Re}_t^{-0.75}\mathrm{e}^{-\left(\frac{\mathrm{Re}_t}{200}\right)^2}\right)\\ f_{\varepsilon 1} &= 1.0\\ f_{\varepsilon 2} &= \left(1-\mathrm{e}^{-\frac{y^*}{3.1}}\right)^2\left(1-0.3\mathrm{e}^{-\left(\frac{\mathrm{Re}_t}{6.5}\right)^2}\right) \end{aligned} \tag{9}$$

The coefficients are chosen as,

$$C_\mu=0.09,\quad C_{\varepsilon 1}=1.5,\quad C_{\varepsilon 2}=1.9,\quad \sigma_k=1.4,\quad \sigma_\varepsilon=1.4. \tag{10}$$

The non-linear model of Lien et al. (1996)

$$\begin{aligned} \tau_{ij} = &-\frac{2}{3}k\delta_{ij}+2\nu_t S_{ij}\\ &-C_1\nu_t T(S_{ik}S_{kj}-\frac{1}{3}S_{kl}S_{kl}\delta_{ij})-C_2\nu_t T(W_{ik}S_{kj}+W_{jk}S_{ki})\\ &-C_3\nu_t T(W_{ik}W_{jk}-\frac{1}{3}W_{kl}W_{kl}\delta_{ij})-C_4\nu_t T^2(S_{ki}W_{lj}+S_{kj}W_{li})S_{kl}\\ &-C_5\nu_t T^2(S_{kl}S_{kl}-W_{kl}W_{kl})S_{ij} \end{aligned} \tag{11}$$

The coefficients are chosen as,

$$C_\mu = 0.667/(1.25 + \xi + 0.9\eta), \quad C_1 = 3/(C_\mu(1,000 + \xi^3))$$
$$C_2 = 15/(C_\mu(1,000 + \xi^3)), \quad C_3 = 19/(C_\mu(1,000 + \xi^3)) \tag{12}$$
$$C_4 = -80C_\mu^2, \quad C_5 = -16C_\mu^2 \quad \xi = \sqrt{2S_{ij}S_{ij}}T, \quad \eta = \sqrt{2W_{ij}W_{ij}}T$$

and

$$f_\mu = (1 - \mathrm{e}^{-0.0198y^*})(1 + 5.29/y^*)$$
$$f_{\varepsilon 1} = 1 + 1.33f_{\varepsilon 2}(P_\mathrm{k} + 2\nu k/y^2)\mathrm{e}^{-0.00375y^{*2}}/P_\mathrm{k} \tag{13}$$
$$f_{\varepsilon 2} = 1 - 0.3\mathrm{e}^{-\mathrm{Re}_t^2} \quad \mathrm{Re}_t = k^2/(\nu\varepsilon), \quad y^* = \sqrt{k}y/\nu$$

The constants are set as,

$$\sigma_k = 1.0, \quad \sigma_\varepsilon = 1.22, \quad C_{\varepsilon 1} = 1.44, \quad C_{\varepsilon 2} = 1.92 \tag{14}$$

The EASM of Speziale (Rokni, 2000; Speziale and Xu, 1995).

$$\tau_{ij} = -\frac{2}{3}k\delta_{ij} + \beta\left[\alpha_1\frac{k^2}{\varepsilon}S_{ij} + \alpha_2\frac{k^3}{\varepsilon^2}(S_{ik}W_{kj} + S_{jk}W_{ki}) - \alpha_3\frac{k^3}{\varepsilon^2}\left(S_{ik}S_{kj} - \frac{1}{3}S_{mn}S_{nm}\delta_{ij}\right)\right] \tag{15}$$

where the coefficients are chosen as

$$\beta = \frac{3(1 + \eta^2)}{3 + \eta^2 + 6\xi^2\eta^2 + 6\xi^2} \tag{16}$$

and

$$\left.\begin{array}{lll} \alpha_1 = \left(\frac{4}{3} - C_1\right)g, & \alpha_2 = 0.5\alpha_1(2 - C_2)g, & \alpha_3 = \alpha_1(2 - C_3)g \\ C_1 = 0.36, & C_2 = 0.40, & C_3 = 1.25 \\ g = \left(\frac{1}{2}C_4 + \frac{P_\mathrm{k}}{\varepsilon} - 1\right)^{-1}, & & C_4 = 6.8 \end{array}\right\} \tag{17}$$

The invariant coefficients are

$$\eta = \frac{1}{2}\frac{\alpha_3}{\alpha_1^2}\frac{k}{\varepsilon}(S_{ij}S_{ij})^{0.5}, \quad \xi = 2\frac{\alpha_2}{\alpha_1^2}\frac{k}{\varepsilon}(W_{ij}W_{ij})^{0.5} \tag{18}$$

The k-ω models. The *k-ω* models use the following transport equations:

$$\frac{\partial k}{\partial t} + \frac{\partial (U_j k)}{\partial x_j} = \frac{\partial}{\partial x_j}\left[\left(\nu + \frac{\nu}{\sigma_k}\right)\frac{\partial k}{\partial x_j}\right] + P_{\mathrm{k}} - \beta^* \omega k \tag{19}$$

$$\frac{\partial \omega}{\partial t} + \frac{\partial (U_j \omega)}{\partial x_j} = \frac{\partial}{\partial x_j}\left[\left(\nu + \frac{\nu}{\sigma_\omega}\right)\frac{\partial \omega}{\partial x_j}\right] + \frac{C_{\omega 1} P_{\mathrm{k}}/k - C_{\omega 2}\omega}{T} \tag{20}$$

where $T = 1/\omega$ is the timescale.

The linear model of Wilcox (1993)

$$\tau_{ij} = 2\nu_t S_{ij} - \frac{2}{3}k\delta_{ij} \tag{21}$$

$$C_\mu = 1.0$$

The coefficients are chosen as,

$$f_\mu = 1.0, \quad \beta^* = 0.09 \quad \sigma_k = 2.0, \quad \sigma_\omega = 2.0 \quad C_{\omega 1} = 5/9, \quad C_{\omega 2} = 3/40 \tag{22}$$

The non-linear model of Larsson (1997)

$$\tau_{ij} = -\frac{2}{3}k\delta_{ij} + 2\nu_t S_{ij} - C_1 \nu_t T(W_{ik}S_{kj} - S_{ik}W_{kj}) \tag{23}$$

The coefficients are chosen as,

$$C_\mu = \frac{1}{\beta^*(6.5 + A_s\alpha)}, \quad C_1 = \frac{2\sqrt{1 - (3C_\mu\xi)^2}}{C_\mu \beta^{*2}(1 + 6\xi\eta)} \tag{24}$$

and

$$A_s = \sqrt{6}\cos(1/3ar\cos(\sqrt{6}\gamma)) \quad C_2 = 15/(C_\mu(1,000 + \xi^3)),$$
$$C_3 = 19/(C_\mu(1,000 + \xi^3)) \quad \xi = \sqrt{2S_{ij}S_{ij}}T, \quad \eta = \sqrt{2W_{ij}W_{ij}}T \tag{25}$$
$$\alpha = \sqrt{S_{ij}S_{ij} + W_{ij}W_{ij}}T/\beta^*, \quad \gamma = S_{ij}S_{jk}S_{ki}T^3/(\beta^*\xi)^3$$

The other coefficients are the same as in the linear model of Wilcox (1993).

Modeling of the turbulent heat fluxes

The turbulent heat flux may be computed using a simple eddy diffusivity (SED) or a generalized gradient diffusion hypothesis (GGDH) model (Rokni, 2000):

SED

$$\overline{\phi' u_j'} = -\frac{\nu_t}{\mathrm{Pr}_t}\frac{\partial \Phi}{\partial x_j} \tag{26}$$

where $\mathrm{Pr}_t = 0.9$.

GGDH

$$\overline{\phi' u_j'} = f_h C_h \frac{k}{\varepsilon}\tau_{ij}\frac{\partial \Phi}{\partial x_i} \tag{27}$$

$$f_h = (1 - \mathrm{e}^{-Ay^*})^2\left(1 + \frac{20.5}{\mathrm{Re}_t}\right) \tag{28}$$

where $C_h = 0.3$, and Re_t and y^* are given by equation (13). A is set to 0.0125 for the non-linear k-ε model and 0.03 for the other non-linear models.

A realizability constraint. A realizability constraint (RZ) (Durbin, 1996) applied on the timescale is used in the calculations:

$$T \le \frac{2}{3}\frac{\alpha}{f_\mu C_\mu \sqrt{C_\alpha S_{ij} S_{ij}}} \tag{29}$$

where $\alpha = 0.6$, $C_\alpha = 2$ for 2D flow, and $C_\alpha = 8/3$ for 3D flow.

Boundary conditions. The governing equations are integrated to the wall and use the following boundary conditions:

$$k_w = 0, \quad \varepsilon_w = \frac{2\nu k}{y^2}, \quad \omega_w = \frac{6\nu}{C_{\omega 2} y^2} \tag{30}$$

where one denotes the first point off the wall, and w denotes the point on the wall.

Numerical solution procedure

The computations for the impingement jets are performed in CFX 4.2. It is a multi-purpose computational code including mathematical models for turbulent fluid flow and heat transfer. The programs use the so-called body-fitted grids, i.e. control volumes of arbitrary shape, to be applicable for any geometry. It is possible for the user to control the discretization scheme, pressure-velocity coupling algorithm, and solution method for the algebraic equation system. For CFX 4.2, the user may add and define transport equations to be solved by the code through the so-called "user-Fortran" subroutines. These routines are read and compiled by the source code to be executed in

parallel with the solution of the equations already implemented in the code, i.e. the continuity, momentum and energy equations.

The implementation, of the turbulence models used in this study into the code CFX 4.2, includes the following five steps:

(1) Setting up scalar transport equations for the turbulence variables k, ε and ω.

(2) Modification of the viscosity used in the code for laminar incompressible flow by addition of a turbulent viscosity.

(3) Addition of non-linear turbulence model terms as source terms to the momentum equations.

(4) Modification of the energy equation: addition of a turbulent diffusivity or addition of a turbulent gradient diffusion heat flux as a source term to the energy equation.

(5) Setting the discretized equation coefficients at the walls to zero and addition of appropriate sources to the transport equations to implement the boundary conditions.

The computations for the 3D ribbed ducts are performed in an in-house multi-block computer code, also based on the finite volume technique. The code uses a collocated mesh arrangement and employs the improved Rhie and Chow interpolation to calculate the velocities at the control volume faces. The SIMPLEC algorithm couples the pressure and velocity. An algorithm based on TDMA is used for solving the equations. Coefficients are determined by the QUICK scheme in all discretized equations.

Under-relaxation is applied for all equations and the source terms of turbulence equations (especially at the starting stage) and the proper values of the relaxation parameters for good convergence behavior were found from some test calculations.

Non-uniform grids were generated, and grid refinement close to the wall was applied. As a low Reynolds number formulation is applied, it is important that the y^+ value of the grid points closest to the wall is of the order of unity. The grids of subsequent calculations have about the same density, and the first grid points are always at a dimensionless distance (y^+) less than 0.5 from the heated walls. In all computations the residuals are reduced about four orders of magnitude from an initial guess.

An investigation of grid dependence was carried out by doubling the number of nodes in each direction (used grid: 160×140) for a first test case. The result was a change less than 5 percent in local heat transfer rates which was considered acceptable (Figure 3). In addition, several successive grid refinements have been carried out in the 3D ribbed duct case to assure negligible effects of the mesh on the solutions. For the validation case with one-sided ribs, $82 \times 82 \times 32$ grid points were used, while for the ducts roughened with V-shaped ribs, $82 \times 56 \times 32$ grid points were used.

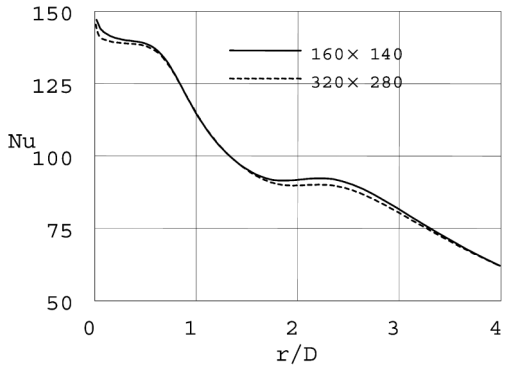

Figure 3.
Grid dependence of local Nusselt number (Re = 23,000, $H/D = 2$)

Results and discussion

Circular impingement jet (case I)

The first case considered is a jet Reynolds number of 23,000 and $H/D = 2$. In Figure 4(a), the calculated local Nusselt number distributions of the linear models are compared to experimental data (Baughn *et al.*, 1991; Yan, 1993). It is clear that the original formulation of the models severely overestimates the heat transfer in the stagnation zone. This is not surprising, because similar linear two-equation models have been found to produce excessive turbulence in stagnating flows (Craft *et al.*, 1993; Kato and Launder, 1993). An investigation of the near wall turbulence intensity along the axis of symmetry confirms these findings (Figure 5(a)) (u' is calculated as $\sqrt{2/3k}$). The k-ω model yields lower stagnation heat transfer rates than the k-ε formulation, which also was found by Larsson (1997). This illustrates that the length scale equation (ε or ω) is of importance and motivates the choice of models in the present investigation. To improve the behavior of the model, a RZ (equation (29)) is applied on the turbulent timescale and the results are included in Figure 4. The constraint was presented by Durbin (1996) using a linear eddy viscosity formulation (V2F-model). It has been found not to affect the solution at equilibrium flow

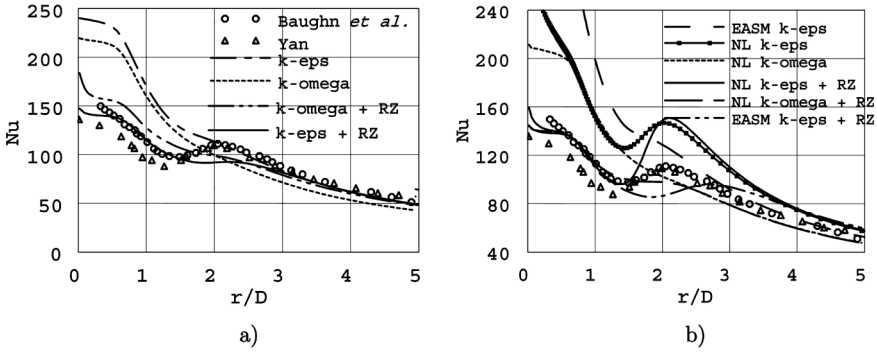

Figure 4.
Influence of RZ on the (a) linear and (b) non-linear models (Re = 23,000 and $H/D = 2$)

conditions and it retains the robustness of the models. However, it must be pointed out that equation (29) includes an *ad hoc* parameter α. The value of this parameter was suggested by Behnia *et al.* (1998), using the V2F turbulence model for the same case as considered here. If the *ad hoc* correction is removed (i.e. $\alpha = 1$), stagnation heat transfer rates will be closer to the results of the original model formulations.

Turning now to the non-linear turbulence models, the results of the same case are given in Figure 4(b). The results are unexpectedly poor for all three models, as the stagnation Nusselt number is calculated at the same or even higher level as the non-realizable linear models. This is very disappointing, as the realizability theory, invoked in the models of Larsson and Lien *et al.* implies a positive effect on the performance of the linear models. Furthermore, the strain dependent non-linear coefficients do not seem to suppress the turbulence generation of the stagnating flow. Only the non-linear k-ω model shows slightly lower stagnation zone heat transfer rates than its linear counterpart. However, if equation (29) is applied on the timescale, much better agreement with experimental data is accomplished, which is also shown in Figure 4(b).

By using non-linear constitutive relationships, it is also possible to allow anisotropic representations of the turbulent heat fluxes. Therefore, a generalized gradient diffusion hypothesis (equation (27)) is applied. The use of such a formulation is based on a proper prediction of the turbulent normal stresses normal to the wall and also the turbulent timescale. An investigation of the models used here for channel flow revealed that satisfactory predictions were not achieved for any of the models. Hence, a Lam-Bremhorst type of damping function (equation (28)) was added to the original GGDH formulation, also suggested by Rokni (2000). The purpose was to make the models fit data extracted from direct numerical simulations (Kasagi *et al.*, 1992) of the temperature field for the channel flow case. Figure 5(b) shows the results of the anisotropic formulation compared to the standard eddy diffusivity concept for the case of Re = 70,000 and $H/D = 2$. In this figure, it is shown that the GGDH formulation in general supplies lower heat transfer rates in the stagnation zone,

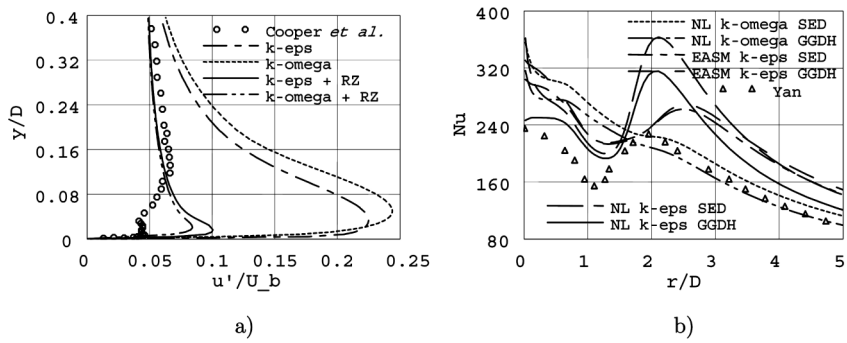

Figure 5.
(a) Influence of RZ on the rms velocity (Re = 23,000 and $H/D = 2$); and
(b) influence of turbulent heat flux formulation on the non-linear models (Re = 70,000 and $H/D = 2$)

which tends to better agreement with the experiments, but does not alter the radial distribution significantly. The strongest effect is seen for the non-linear k-ε model. As expected, the anisotropic formulation predicts a significant turbulent heat flux in the radial direction despite a very small temperature gradient, which is not possible using the eddy diffusivity approach. But as the heat flux varies rather slowly in this direction (except in the stagnation zone), the energy balance is only moderately affected which leads to similar Nusselt number distributions.

A circular impingement jet issued into a crossflow (case II)

The calculated Nusselt number along the x-axis at the bottom wall is compared to the experimental data in Figure 6 for crossflow to jet ratios $M = 0.2$, 0.1.

For the case of $M = 0.2$, the computed heat transfer is significantly higher than the experimental values, and the profile shape is not reproduced very well. As the crossflow is reduced (case $M = 0.1$) this quantitative difference between experiments and calculations is reduced. The zero crossflow case is predicted quite well and the additional experimental data (Lee and Lee, 1999) (Re = 30,000) are included for comparison. The presence of crossflow significantly reduces the heat transfer in the experiments. This is not seen in the calculated results, as the intermediate crossflow case exhibits the highest heat transfer levels. The reason may be improper turbulence modeling and a too high turbulence generation associated with the jet and crossflow interaction.

A picture of the rotating motions that is generated in the wake of the jet is also included in Figure 7. These vortices will distort the jet cross-section into a kidney-shape, which leaves a footprint on the shape of the stagnation zone heat transfer for $M = 0.2$ in the simulations. The same wall heat transfer shape has been detected in the corresponding experiments, but at a lower crossflow to jet ratio.

3D ribbed ducts (case III)

Figure 8(a) shows the flow structure in a 3D ribbed duct. In the simulation results, the main stream flow turns toward the side wall in the front of the next

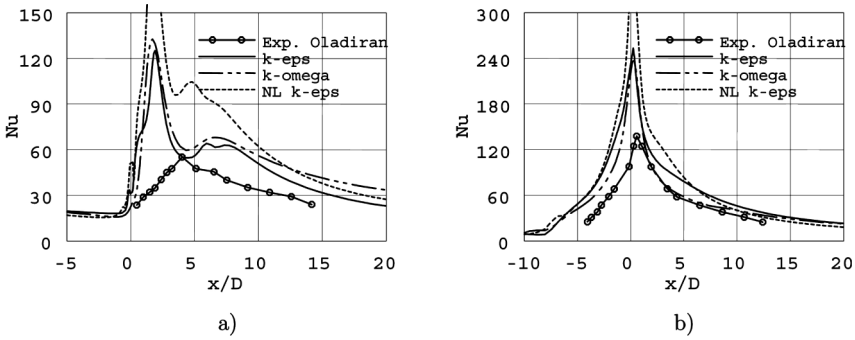

Figure 6.
Nusselt number along x-axis for (a) $M = 0.2$, and (b) $M = 0.1$

rib, and it is also true for flow behind the rib very close to the side wall. All these phenomena can also be observed in the experimental data.

Experimental investigations proved the existence of a large vortex cell in each half-cross-sectional plane of a one-sided ribbed duct and on top of a rib. This can also be clearly observed in the present simulation. The Nusselt number was measured at the symmetry line. As shown in Figure 8(b), it is somewhat over-predicted, due to a slight over-prediction of turbulent fluctuating velocity. In general, the present simulations are in pretty good agreement with the experiments, therefore, the solver is employed in the following study for V-shaped ribbed ducts.

Table I shows the goodness factor for 45° V-shaped ribs pointing up- and downstream. This overall factor is closely related to the heat transfer coefficient, because the rib direction has little effect on the friction factor. It can be observed clearly that the 45° V-shaped ribs pointing upstream performed much better than 45° V-shaped ribs pointing downstream, for the two

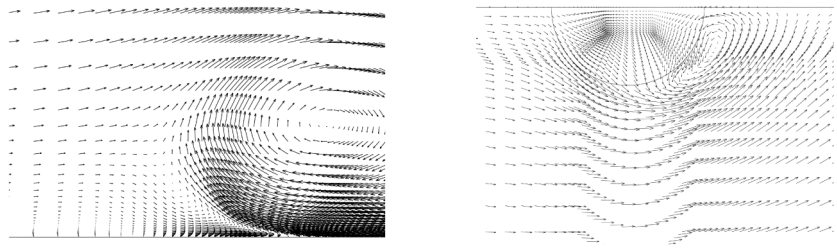

Figure 7.
Flow field near bottom wall in front of the jet at (a) $z = 0$; and (b) $y = 5.5$ planes ($M = 0.2$)

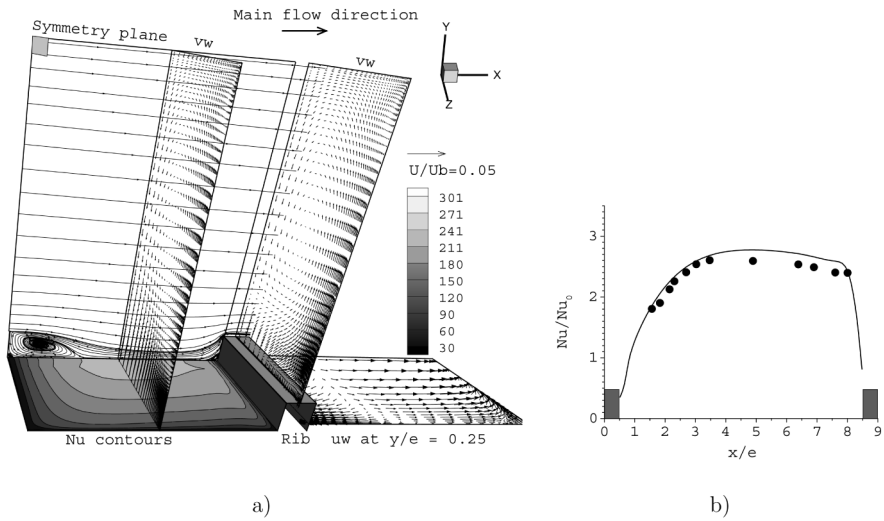

Figure 8.
Heat and fluid flow in periodic fully developed flow in one-sided-ribbed duct. (a) Flow structure; and (b) normalized Nusselt number at the ribbed wall symmetry line, in comparison with Rau *et al.* (1998) (•)

simulated Reynolds numbers. This can be explained from both the favorable secondary flow induced by the angled ribs and vortex stretching near the ribbed side-wall.

The higher heat transfer coefficient on the ribbed side wall for the V-shaped ribs pointing upstream can be explained by the vortex line stretching, as shown in Figure 9. As discussed by Olsson and Sundén (1998), the vortex line is bent to a V-shaped form similar to the ribs if the vortex line is close to the wall. The vortex line will be stretched and the vorticity amplified by the velocity gradients in the vicinity of the ribs. Consequently, the vortex line now has both axial and spanwise components. The axial component is associated with the secondary flow, while the spanwise component has similar behavior as the original vortex line. For the V-shaped ribs pointing upstream, the axial vorticity components (Figure 9(b)) will act as an inflow pair of vortices resulting in thinning of the boundary layer and enhancing the heat transfer on the ribbed side-wall. For the V-shaped ribs pointing downstream, an outflow vortex pair (Figure 9(a)) will occur and the boundary layer thickness is increased, which decreases the local heat transfer.

Conclusions

Our recent investigations show that linear and non-linear two-equation turbulence models can be used for impinging jet heat transfer predictions with reasonable success. However, the computational results also suggest that an

Reynolds number	Downstream V-shaped ribs	Upstream V-shaped ribs
15,000	0.255	0.381
25,000	0.155	0.200

Table I.
Comparison of goodness factor (j/f)

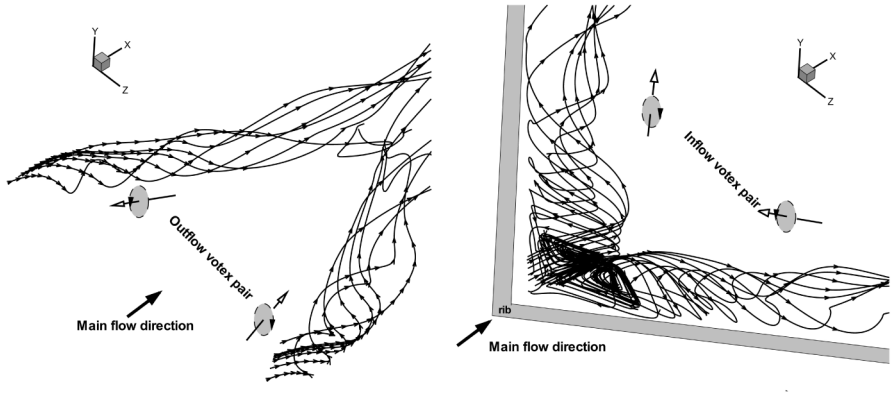

Figure 9.
Vortex pair from the present simulations. (a) V-shaped ribs pointing downstream; and (b) V-shaped ribs pointing upstream

application of a realizability constraint is necessary to avoid overprediction of the stagnation point heat transfer coefficients. For situations with combined forced convection and impingement cooling it was revealed that as the crossflow is squeezed under the jet, the heat transfer coefficient is reduced. In addition, inline V-shaped 45° ribs pointing upstream performed superior compared to those pointing downstream and transverse ribs. This is mainly because of the secondary flow induced by the angled ribs. Such results are relevant as the disagreement between various experiments is analyzed.

References

Abe, K., Kondoh, T. and Nagano, Y. (1994), "A new turbulence model for predicting fluid flow and heat transfer in separating and reattaching flows – I. Flow field calculations", *Int. J. Heat Mass Transfer*, Vol. 37 No. 1, pp. 139-51.

Ashforth-Frost, S. and Jambunathan, K. (1996), "Numerical prediction of semi-confined jet impingement and comparison with experimental data", *Int. J. Numerical Meth. Fluids*, Vol. 23, pp. 295-306.

Baughn, J., Hechanova, A. and Yan, X. (1991), "An experimental study of entrainment effects on the heat transfer from a flat surface to a heated circular impinging jet", *ASME J. Heat Transfer*, Vol. 113, pp. 1023-5.

Behnia, M., Parneix, S. and Durbin, P.A. (1998), "Prediction of heat transfer in an axisymmetric turbulent jet impinging on a flat plate", *Int. J. Heat Mass Transfer*, Vol. 41, pp. 1845-55.

Craft, T.J., Graham, L.J.W. and Launder, B.E. (1993), "Impinging jet studies for turbulence model assessment – II. An examination of the performance of four turbulence models", *Int. J. Heat Mass Transfer*, Vol. 36, pp. 2685-97.

Durbin, P.A. (1996), "On the k-ε stagnation point anomaly", *Int. J. Heat Fluid Flow*, Vol. 17, pp. 89-90.

Han, J.C., Zhang, Y.M. and Lee, C.P. (1991), "Augmented heat transfer in square channels with parallel, crossed, and V-shaped angled ribs", *ASME J. Heat Transfer*, Vol. 113, pp. 590-6.

Heyerichs, K. and Pollard, A. (1996), "Heat transfer in separated and impinging turbulent flows", *Int. J. Heat Mass Transfer*, Vol. 39 No. 12, pp. 2385-400.

Hosseinalipour, S.M. and Mujumdar, A.S. (1995), "Comparative evaluation of different turbulence models for confined impinging and opposing jet flows", *Numerical Heat Transfer Part A*, Vol. 28, pp. 647-66.

Iacovides, H. and Raisee, M. (1999), "Recent progress in the computation of flow and heat transfer in internal cooling passages of turbine blades", *Int. J. Heat and Fluid Flow*, Vol. 20 No. 3, pp. 320-8.

Jang, Y., Chen, H. and Han, J. (2001), "Computation of flow and heat transfer in two-pass channels with 60 deg ribs", *ASME J. Heat Transfer*, Vol. 123, pp. 563-75.

Kasagi, N., Tomita, Y. and Kuroda, A. (1992), "Direct numerical simulation of passive scalar field in a turbulent channel flow", *ASME J. Heat Transfer*, Vol. 114, pp. 598-606.

Kato, M. and Launder, B.E. (1993), "The modelling of turbulent flow around stationary and vibrating cylinders", *Proceedings of the 9th Symposium on Turbulent Shear Flows*, Kyoto, pp. 1041-6.

Larsson, J. (1997), "Two-equation turbulence models for turbine blade heat transfer simulations", *Proc. 13th ISABE Conf.*, ISABE Paper 97-7163, Vol. 2, pp. 1214-22.

Lee, J. and Lee, S.J. (1999), "Stagnation region heat transfer of a turbulent axisymmetric jet impingement", *Exp. Heat Transfer*, Vol. 12, pp. 137-56.

Lien, F.S., Chen, W.L. and Leschziner, M.A. (1996), "Low-Reynolds-number eddy-viscosity modelling based on non-linear stress-strain/vorticity relations", *Proc. 3rd Symp. Engineering Turbulence Modelling and Measurements*, Crete, Greece.

Lytle, D. and Webb, B. (1994), "Air jet impingement heat transfer at low nozzle-plate spacings", *Int. J. Heat Mass Transfer*, Vol. 37, pp. 1687-97.

Oladiran, M.T. "The effect of nozzle inclination on heat transfer in jet impingement systems", (1981), PhD thesis, Cranfield Institute of Technology, UK.

Olsson, C.O. and Sundén, B. (1998), "Experimental study of flow and heat transfer in rib-roughened rectangular channels", *Experimental Thermal and Fluid Science*, Vol. 16 No. 4, pp. 349-65.

Rau, M., Cakan, Moeller, M.D. and Arts, T. (1998), "The effect of periodic ribs on the local aerodynamics and heat transfer performance of a straight cooling channel", *ASME J. Turbomachinery*, Vol. 120, pp. 368-75.

Rokni, M. (2000), "A new low-Reynolds version of an explicit algebraic stress model for turbulent convective heat transfer in ducts", *Numerical Heat Transfer Part A*, Vol. 37 No. 3, pp. 331-63.

Saidi, A. and Sundén, B. (2000), "Numerical simulation of turbulent convective heat transfer in square ribbed ducts", *Numerical Heat Transfer, Part A*, Vol. 38 No. 1, pp. 67-88.

Seyedin, S.H., Hasan, M. and Mujumdar, A.S. (1995), "Turbulent flow and heat transfer from confined multiple impinging slot jets", *Numerical Heat Transfer Part A*, Vol. 27, pp. 35-51.

Speziale, C.G. and Xu, X.H. (1995), "Towards the development of second-order closure models for non-equilibrium turbulent flows", *Proc. 10th Symp. Turb. Shear Flows*, Pennsylvania State University, USA, Vol. 23, pp. 7-12.

Taslim, M.E., Liu, T. and Kercher, D.M. (1996), "Experimental heat transfer and friction in channels roughened with angled, V-shaped, and discrete ribs on two opposite walls", *ASME J. Turbomachinery*, Vol. 118 No. 1, pp. 20-8.

Tzeng, P.Y., Soong, C.Y. and Hsieh, C.D. (1999), "Numerical investigation of heat transfer under confined impinging turbulent slot jets", *Numerical Heat Transfer Part A*, Vol. 35, pp. 903-24.

Wilcox, D.C. (1993), "Turbulence modelling for CFD", DCW Industries Inc., La Cañada, USA.

Yan, X. (1993) "A preheated-wall transient method using liquid crystals for measurement of heat transfer on external surfaces and in ducts", PhD thesis, University of California, Davis.